ACCOUNTS of chemical research

pubs.acs.org/accounts Article

Theory of Long-Lived Room-Temperature Phosphorescence in Organic Aggregates

Qian Peng, Huili Ma, and Zhigang Shuai*

Cite This: *Acc. Chem. Res.* 2021, 54, 940−949 Read Online

ACCESS | Metrics & More | Article Recommendations

CONSPECTUS: Room-temperature phosphorescence (RTP) with a long afterglow from purely organic molecular aggregates has recently attracted many investigations because traditionally only inorganic and transition-metal complexes can emit phosphorescence at room temperature. Purely organic molecules can exhibit phosphorescence only at cryogenic temperatures and under inert conditions in solution. However, recently, a number of organic compounds have been found to demonstrate bright RTP upon aggregation, sometimes with a remarkable morphology dependence. We intended to rationalize such aggregation-induced organic RTP through theoretical investigation and quantum chemistry calculations by invoking intermolecular interaction effects. And we have identified the molecular descriptors for the molecular design of RTP materials.

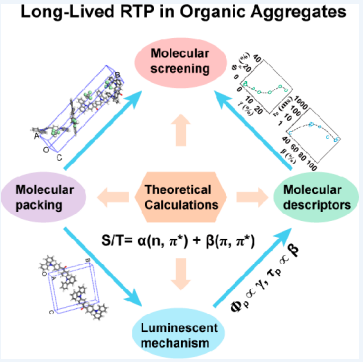

In this Account, we started with the proposition of the mechanism of intermolecular electrostatic-interaction-induced RTP at the molecular level by using molecular dynamics simulations, hybrid quantum mechanics, and molecular mechanics (QM/MM) coupled with the thermal vibration correlation function (TVCF) formalism we developed earlier. The effective intermolecular electrostatic interactions could stem from a variety of interactions in different organic RTP crystals, such as hydrogen bonding, π−halogen bonding, anion−π^+ interaction, and d−pπ bonds and so forth. We find that these interactions can change the molecular orbital compositions involved in the lowest-lying singlet and triplet excited states that are responsible for phosphorescence, either through facilitating intersystem crossing from the excited-state singlet to the triplet and/or suppressing the nonradiative decay process from the lowest triplet to the ground state. This underlying RTP mechanism is believed to be very helpful in systematically and comprehensively understanding the aggregation/crystal-induced persistent organic RTP, which has been applied to explain a number of experiments.

We then propose the molecular descriptors to characterize the phosphorescence efficiency and lifetime, respectively, derived from fundamental photophysical processes and requirements to obey the El-Sayed rule and generate phosphorescence. For a prototypical RTP system consisting of a carbonyl group and π-conjugated segments, the excited states can be regarded as an admixture of n → π^* (with portion α) and π → π^* (with portion β). The intersystem crossing (ISC) rate of S_1 → T_n is mostly governed by the modification of the product of α and β, and the nonradiative rate of T_1 → S_0 is determined by the β value of T_1. Thus, we employ $\gamma = \alpha \times \beta$ and β to describe the phosphorescence efficiency and lifetime, respectively, which have been successfully applied in the molecular design of efficient and long-lived RTP systems in experiments. The molecular descriptors outlined in this Account, which are easily obtained from simple quantum chemistry calculations, are expected to play important roles in the machine-learning-based molecular screening in the future.

KEY REFERENCES

- Ma, H.; Shi, W.; Ren, J.; Li, W.; Peng, Q.; Shuai, Z. Electrostatic Interaction-Induced Room-Temperature Phosphorescence in Pure Organic Molecules from QM/MM Calculations. *J. Phys. Chem. Lett.* **2016**, *7*, 2893−2898[1] *The intermolecular electrostatic interaction was first introduced to elucidate the enhancement in phophorescence oscillator strength through analyzing the transition compositions of the low-lying singlet states, revealing the boosted organic room-temperature phosphorescence (RTP) in the crystal from solution.*
- Ma, H.; Yu, H.; Peng, Q.; An, Z.; Wang, D.; Shuai, Z. Hydrogen Bonding-Induced Morphology Dependence of Long-Lived Organic Room-Temperature Phosphorescence: A Computational Study. *J. Phys. Chem. Lett.* **2019**, *10*, 6948−6954.[2] *The model is expanded to explain*

Received: September 1, 2020
Published: December 21, 2020

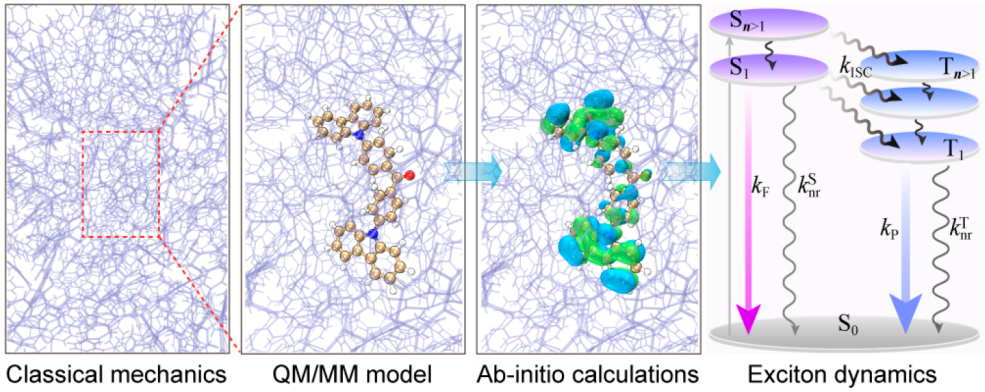

Figure 1. Computational scheme for RTP properties in organic compounds. The aggregate morphology is generated by molecular dynamics (MD) simulations and the crystalline structure coming from the experimental X-ray structure and/or from the combined polymorph predictor and periodic DFT optimization. The relevant Jablonski diagram is shown in the right panel.

the hydrogen bonding interaction impacts on the transition compositions of the low-lying triplet states, elucidating the morphology dependence of RTP in organic aggregates caused by the suppressed triplet nonradiative decays.

- Zhao, W.; He, Z.; Lam, J.; Peng, Q.; Ma, H.; Shuai, Z.; Bai, G.; Hao, J.; Tang, B. Rational Molecular Design for Achieving Persistent and Efficient Pure Organic Room-Temperature Phosphorescence. *Chem.***2016**, *1*, 592−602.[3] *The underlying relationship is established between the proportion of n and π orbitals and the rates of intersystem crossing and phosphorescence decay, and accordingly a series of full-color pure organic phosphors are designed and synthesized with an efficiency of up to 36.0% and a long lifetime of 0.23 s under ambient conditions.*
- Ma, H.; Peng, Q.; An, Z.; Huang, W.; Shuai, Z. Efficient and Long-Lived Room-Temperature Organic Phosphorescence: Theoretical Descriptors for Molecular Designs. *J. Am. Chem. Soc.* **2019**, *141*, 1010−1015.[4] *The model is extended to build a pair of molecular descriptors γ and β to positively describe the phosphorescence quantum efficiency and lifetime, respectively.*

1. INTRODUCTION

Room-temperature phosphorescence (RTP) with a long afterglow from purely organic molecular aggregates has recently attracted a great number of investigations from both academic and industrial interests due to its potential applications in biological imaging, digital encryption, optoelectronic devices, and so on.[5−9] Traditionally, only inorganic and transition-metal complexes can emit phosphorescence at room temperature, and phosphorescence from purely organic molecules can be observed only at cryogenic temperatures and under inert conditions in solution,[10] except that an unusually weak afterglow was observed at room temperature for some crystalline organic compounds in 1970s.[11,12] However, recently, a number of organic compounds have been found to exhibit highly efficient RTP in the aggregates,[13−18] depending on the morphology, often in the crystalline phase.[5,19,20] Moreover, the same molecule with a different packing structure can display quite different RTP behavior.[21−23] Some compounds exhibit quite long RTP lifetimes of hundreds of milliseconds or even as long as seconds but with a low quantum efficiency of less than 5% in crystals,[10,14] and some compounds have a strong RTP but short lifetimes of microseconds.[13] Understanding the underlying mechanism of the RTP in an organic aggregate is essential to the molecular design of efficient and long-lifetime RTP molecules. In organic aggregates, the intermolecular interactions are rich, including π−π, cation−π, anion−π^+, H−π/CH−π, π_{cation}−π, hydrogen bonding, halogen bonding, and π−halogen bonding, and the nature of forces varies, including electrostatic, dispersion, exchange (repulsion), and induction (polarization).[24−26] The interactions can change the molecular geometrical/electronic structures and affect the excited-state energy dissipation pathways.[1−3,5,27−33] These interactions and the molecular excited-state structures are difficult to characterize in experiments. Thus, the theoretical understanding and computational characterization become imperative.[34]

In this Account, we first reveal the mechanisms of aggregation-induced RTP through a computational study by combining molecular dynamics (MD), quantum mechanics, and molecular mechanics (QM/MM) and carrying out excited-state dynamic calculations (Figure 1). We then proposed a molecular design strategy via adjusting the electronic configuration (n, π*) and (π, π*) components to jointly enhance the efficiency and lifetime, and finally we suggested a pair of molecular descriptors to characterize the efficiency and lifetime of the molecular model consisting of an n group with a lone pair of electrons and π group, which has been successfully demonstrated in several experimental applications.

2. MECHANISM OF RTP IN AGGREGATION

From the Jablonski diagram in Figure 1, photophosphorescence occurs along the pathway $S_1 \rightarrow T_n \rightarrow T_1 \rightarrow S_0$. The notations of the various rates are the following: k_F and $k_{nr}^{S_1}$ are the radiative decay and nonradiative decay (internal conversion) rate constants from S_1 to S_0, respectively. k_{ISC} is the intersystem crossing rate constant from S_1 to T_n. And k_P and $k_{nr}^{T_1}$ are the radiative and nonradiative decay rate constants from T_1 to S_0. We assume the internal conversion from higher to lower excited states to be fast enough. Then, the phosphorescence quantum efficiency and lifetime can be written as

$$\Phi_P = \Phi_{ISC}\phi_P = \Phi_{ISC}k_P\tau_P \quad (1)$$

$$\tau_P = 1/(k_P + k_{nr}^{T_1}) \quad (2)$$

Here, Φ_{ISC} is the quantum yield of triplet state $\Phi_{ISC} = k_{ISC}/(k_F + k_{nr}^{S_1} + k_{ISC})$. These rate constants can be calculated through the thermal vibration correlation function (TVCF) formalism

https://dx.doi.org/10.1021/acs.accounts.0c00556
Acc. Chem. Res. 2021, 54, 940−949

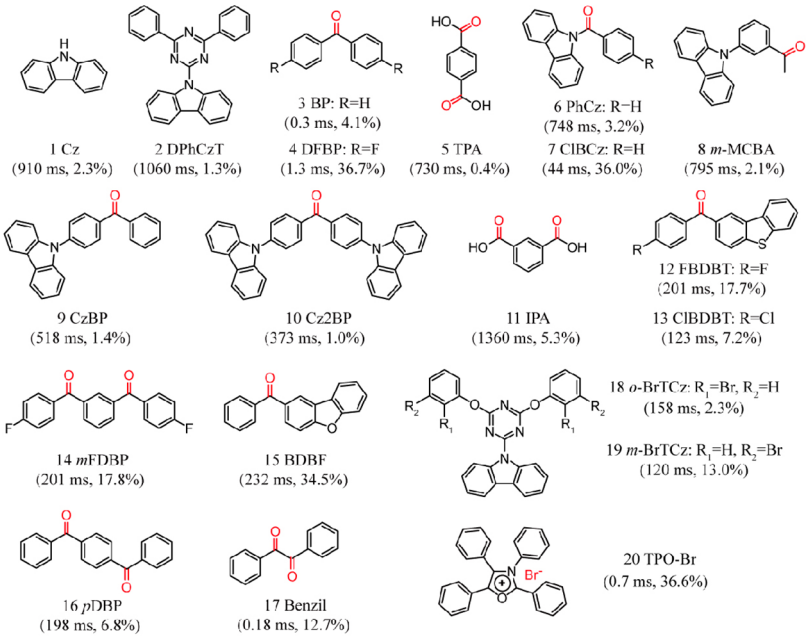

Figure 2. Chemical structure of organic RTP compounds along with the phosphorescence lifetime and quantum efficiency in parentheses.

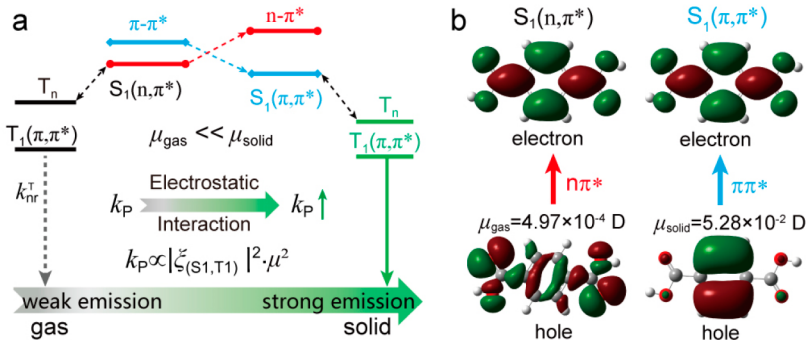

Figure 3. Energy level and natural transition orbitals (NTO) of the excited states for molecule **5** in the gas and solid phases. Reproduced with permission from ref 1. Copyright 2016 American Chemical Society.

developed by our group, coupled with first-principles electronic structures from the quantum chemistry package.[1,2,29] The intermolecular interaction effects are investigated at the quantum mechanics/molecular mechanics (QM/MM) level, namely, the excited-state structure and dynamics are calculated at the QM level under the influence of the surrounding molecules treated at the MM level. We have applied this computational protocol to investigate the RTP mechanism for the compounds listed in Figure 2, in close collaboration with several experimental groups, to rationalize the mechanism of RTP and then to propose molecular design strategies, which have been rationalized in refs 1, 2, 20, 21, 28, 32, 33, and 35.

2.1. Electrostatic-Interaction-Enhanced k_P through Making S_1 Brighter

The first example we showed here is terephthalic acid (TPA) (**5** in Figure 2), which was reported to exhibit RTP upon crystallization.[35] It serves as our prototypical system to unravel the mechanism of crystallization-induced RTP. We optimized the geometrical and electronic structures of the low-lying singlet/triplet states by the (TD)B3LYP/CC-PVDZ approach as implemented in the TURBOMOLE 6.5 package and calculated the excitation energy using the state-of-the-art second-order perturbation theory based on the complete active space self-consistent field (CASPT2/ANO-RCC-PVDZ) with active space (8e, 8o)[36] in the MOLCAS package[37] and the hybrid CASPT2 (8e, 8o)/AMBER with ANO-RCC-PVDZ by interfacing MOLCAS and TINKER[38] packages for molecule **5** in the gas and crystalline phases, respectively.

It is found from the nature of the low-lying excited states in Figure 3 that the S_1 state is formed by the transition from the n orbital to the π^* orbital (n, π^*) while the S_2 state is formed by the transition from the π orbital to the π^* orbital (π, π^*) for TPA in the gas phase. The n orbital is more easily affected by electrostatic forces owing to the charge concentrated on the oxygen, which gives a separation of charge that differs from that of the π orbital with uniform charge distributions (Figure 3b). When going to the solid phase, the n orbital is stabilized greatly while the π orbital is affected slightly by the intermolecular electrostatic interaction, which results in a large increment of the ^{1}(n, π^*) state and a slight variation of the ^{1}(π, π^*) state in energy. Namely, upon crystallization, the ^{1}(n, π^*) state is increased to 5.05 eV from 4.81 eV while the ^{1}(π, π^*) state is reduced to 4.76 eV from 4.99 eV in the gas phase. Hence, crystallization converts the nature of the S_1 state from ^{1}(n, π^*) to ^{1}(π, π^*). As a consequence, the corresponding electric transition dipole (π) of the S_1 state is sharply enhanced

https://dx.doi.org/10.1021/acs.accounts.0c00556
Acc. Chem. Res. 2021, 54, 940−949

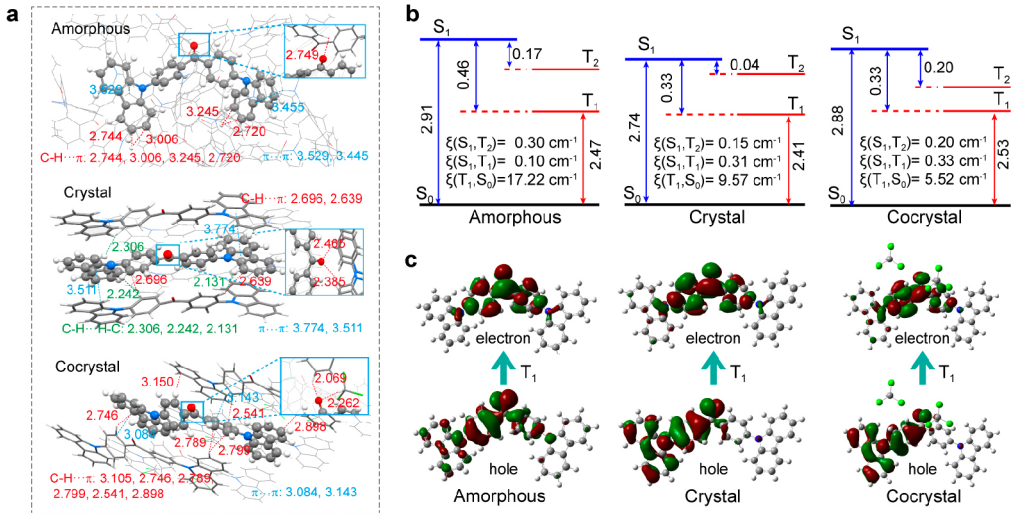

Figure 4. (a) Molecular packing with distance (angstroms). (b) Energy levels and SOC of the low-lying states. (c) NTOs of the T_1 state for Cz2BP in amorphous, crystalline, and cocrystalline phases. Reproduced from ref 2. Copyright 2019 American Chemical Society.

Table 1. Calculated k_F and k_{ISC} of $S_1 \rightarrow T_n$ (n = 1, 2); k_P, $k_{nr}^{T_1}$, and Quantum Efficiency $\phi_P = k_P/(k_P + k_{nr}^{T_1})$ of $T_1 \rightarrow S_0$; and RTP Lifetime $\tau_P = 1/(k_P + k_{nr}^{T_1})$ for Molecule 10 in Amorphous (A0−A4), Crystal, and Cocrystal Forms (T = 300 K), with the Experimental Lifetime Also Listed as a Comparison

	$S_1 \rightarrow S_0$	$S_1 \rightarrow T_2$	$S_1 \rightarrow T_1$	$T_1 \rightarrow S_0$					
						ϕ_P (%)		τ_P (ms)	
T = 300 K	k_F (s^{-1})	k_{ISC} (s^{-1})	k_{ISC} (s^{-1})	K_P (s^{-1})	$k_{nr}^{T_1}$ (s^{-1})	cal.	exp.	cal.	exp.
A0	3.57×10^7	2.70×10^7	1.36×10^6	4.47×10^1	1.87×10^6	0.002	RTP ×	0.02	
A1	1.56×10^7			3.06×10^1	6.67×10^4	0.046	RTP ×	0.46	
A2	2.76×10^7			4.71×10^1	2.77×10^5	0.017	RTP ×	0.17	
A3	5.12×10^7			4.97×10^1	1.16×10^6	0.004	RTP ×	0.04	
A4	2.36×10^7			4.78×10^1	1.30×10^6	0.004	RTP ×	0.04	
crystal	4.43×10^7	4.14×10^6	2.21×10^7	3.15×10^1	5.51×10^3	0.57	RTP ×	5.68	
cocrystal	7.03×10^7	3.96×10^7	3.24×10^6	1.58	6.03	20.76	RTP √	208	353

by 2 orders of magnitude from $\mu_{gas} = 4.97 \times 10^{-4}$ to $\mu_{solid} = 5.28 \times 10^{-2}$ D upon aggregation. These eventually enhance the phosphorescence rate constant by almost 4 orders of magnitude according to the approximate relationship of $k_P \propto |\xi_{(S1,T1)}|^2 \cdot \mu^2$ where the S_1 state serves as the most dominant intermediate state with the smallest energy gap and significant SOC between the S_1 and T_1 states.[39] Meanwhile, T_1 maintains its $^3(\pi, \pi^*)$ character in both the gas phase and solid phase, which suggests that there would not be significant change for the nonradative decay rate of T_1. Therefore, the RTP of molecule **5** in the crystalline phase is generated mainly because the intermolecular electrostatic interaction converts the S_1 from transition-dipole-forbidden $^1(n, \pi^*)$ to strongly dipole-allowed $^1(\pi, \pi^*)$, which significantly enhances the k_P.

This mechanism of electrostatic interaction-activated efficient phosphorescence decay through bright S_1 not only helps to understand the RTP behaviors of some compounds containing dark $^1(n, \pi^*)$ or complete charge-transfer excited states but can be applied in designing efficient RTP through varying substitutions of aromatic molecules to increase the transition dipole moment of single states to accelerate k_P.[40]

2.2. Hydrogen-Bonding-Induced RTP through Suppressing the $k_{nr}^{T_1}$−Vibronic Decoupling Effect

4,4′-Bis(9*H*-carbazol-9-yl)methanone (Cz2BP, **10** in Figure 2) emits persistent RTP in a cocrystal consisting of chloroform (TCM) but not in an amorphous form or in a crystal,[22,41] demonstrating interesting morphology-dependent RTP behavior.[2] The aggregate structures for the amorphous and crystalline phases are built first at the level of classical mechanics. The amorphous aggregate was generated by molecular dynamics (MD) simulations with the general amber force field (GAFF) for 20 ns with a time step of 2 fs and a configuration storage period of 2 ps for data analysis for a cubic box of 15 × 15 × 15 nm^3. Typically, the equilibrium condition is reached after 10 ns, and we extracted the configurations in the last 2 ns from five trajectories as an amorphous structure. The crystalline aggregate was predicted by combining the polymorph predictor and periodic DFT optimization with PBE-D3(bj) in close comparison with the experimental X-ray powder diffraction (XRPD).[22] In addition, the experimental cocrystal conformation was optimized at the PBE-D3(bj) level for comparison. Considering the obtained morphology in Figure 4a, we find that the packing becomes denser with density increasing from 1.158 to 1.324 to 1.505 g/cm^3 and that the major peak of the averaged radial distribution functions (RDFs) decrease from ca. 2.715 to 2.385/2.465 to 2.069/2.262 Å from amorphous to crystal to cocrystal. More significantly, the intermolecular hydrogen bonding is notably strengthened with the C═O···H−C distance shortened from 2.977 to 2.488 Å in five representative amorphous phases, from 2.465 to 2.385 Å in the crystal, and finally from 2.069 to 2.262 Å in the cocrystal.

https://dx.doi.org/10.1021/acs.accounts.0c00556
Acc. Chem. Res. 2021, 54, 940−949

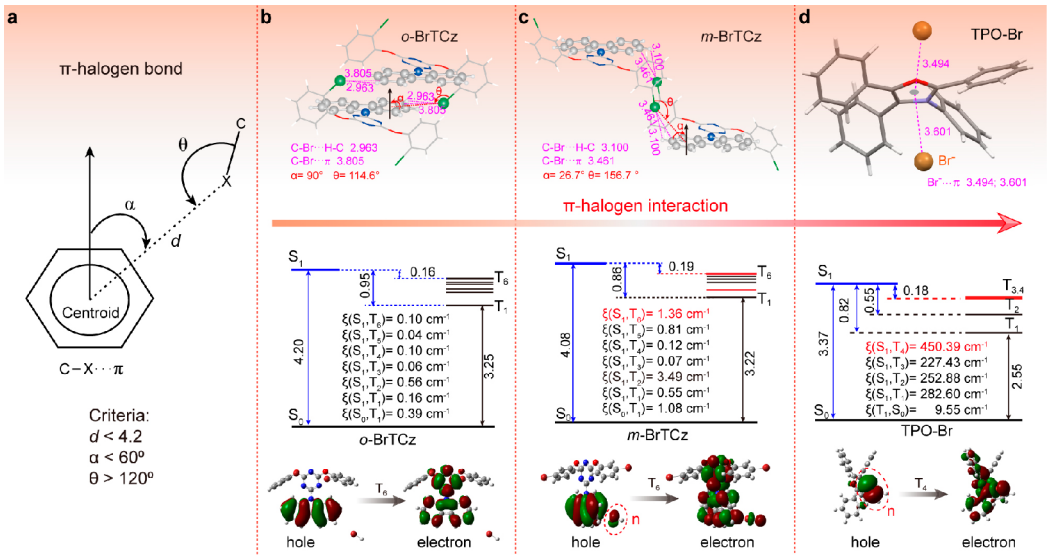

Figure 5. (a) π−halogen bond in an organic molecule and molecular packing and intermolecular interactions, energy levels, SOCs, and NTOs of molecules (b) **18**, (c) **19**, and (d) **20**. Reproduced with permission from ref 32. Copyright 2018 John Wiley and Sons. Reproduced with permission from ref 33. Copyright 2018 Springer Nature.

Then, we extract a big cluster from the aggregates to perform the QM/MM calculation with TDDFT/B3LYP/6-31G(d)/GAFF for the geometrical and electronic structures of the low-lying excited states of molecule **10** in three phases through ChemShell 3.5[42] packages interfacing Turbomole 6.5[36] with DL_POLY,[43] and the spin−orbit coupling (SOC) constant is calculated with the Beijing density functional (BDF) program.[44,45] It is interesting to find that the nature of the T_1 state strongly depends on the morphology because of the mixed (n, π^*) and (π, π^*) character. Namely, the (π, π^*) component is 59.8% amorphous but increased to 88.6% in the crystal and to 94.6% in the cocrystal, which results in the decrease in SOC coefficients $\zeta(T_1, S_0)$ from 17.22 cm^{-1} in the amorphous state, from 9.57 cm^{-1} in the crystal, and from 5.52 cm^{-1} in the cocrystal. Contrary to T_1, the S_1 and T_2 states have similar electronic configurations of (π, π^*) character and give almost unchanged weak SOCs with $\zeta(T_1, S_1)$ and $\zeta(T_2, S_1)$ values of less than 0.33 cm^{-1} in the three phases. These suggest that $k_{nr}^{S_1}$ and k_F of $S_1 \rightarrow S_0$ and k_{ISC} of $S_1 \rightarrow T_n$ would be less affected but that $k_{nr}^{T_1}$ and k_P of $T_1 \rightarrow S_0$ would be remarkably influenced owing to the participation of variable T_1 in different phases.

The rate constants of the involved processes were quantitatively calculated by using the TVCF method[46] as implemented in our home-built MOMAP (MOlecular MAterials Property Prediction) program,[47] listed in Table 1. We have developed TVCF based on Fermi's golden rule with a nonadiabatic coupling term (consisting of all of the molecular vibrational modes), an electric transition dipole term, and the SOC term as perturbations to evaluate the nonradiative, radiative, and intersystem crossing rate constants, respectively, between molecular electronic states within a time-dependent formalism by virtue of a fast-Fourier transformation technique.[39] TVCF has been extensively applied for the evaluation of light-emitting efficiency, the underlying mechanism of the aggregation-induced emission, and the room-temperature phosphorescence in an efficient and reliable way.[1,2,28−31] From Table 1, the k_{ISC} of $S_1 \rightarrow T_2/T_1$ and the k_F of $S_1 \rightarrow S_0$ are all insensitive to morphology, ~10^6−10^7 s^{-1} in all three phases, which is consistent with the similar electronic structure features of S_1 and T_2. The k_P of $T_1 \rightarrow S_0$ decreases by 1 order of magnitude to 1.58 s^{-1} in the cocrystal from 4.78 × 10^1 and 3.15 × 10^1 s^{-1} in the other aggregates. Most strikingly, the $k_{nr}^{T_1}$ of $T_1 \rightarrow S_0$ is sharply reduced by 3−6 orders of magnitude to 6.03 s^{-1} in the cocrystal from 1.87 × 10^6 in amorphous A0 (with similar results for A1−A4) and 5.51 × 10^3 s^{-1} in the crystal. Consequently, a highly efficient phosphorescence of ϕ_P = 20.76% in the cocrystal is predicted, in sharp contrast to ϕ_P< 0.04% in the amorphous structure and ϕ_P < 0.57% in the crystal, according to the equation $\phi_P = k_P/(k_P + k_{nr}^{T_1})$. The predicted RTP lifetime of 208 ms is in good agreement with the experimental value of 353 ms.

To determine the underlying reason for such a big drop in $k_{nr}^{T_1}$ in the cocrystalline phase, we analyzed the vibronic couplings in detail. It is found that the C═O bond stretching is the most important mode which causes the large vibrational relaxation in the $T_1 \rightarrow S_0$ nonradiative decay process. The C═O bond length modification between the T_1 and S_0 states is shortened by 0.092, 0.064, and 0.043 Å from amorphous to crystal to cocrystal phases, respectively. Such sizable decreases in the bond length are ascribed to the decreased n-electron density at the O atom site. The C═O stretching vibrational frequency undergoes a red shift from 1740.93 to 1736.21 to 1711.36 cm^{-1} for the three phases with T_1 geometry. The reorganization energy λ from the relaxation of this bond is greatly reduced from 1888.46 cm^{-1} in the amorphous phase to 717.24 in the crystal to 186.67 cm^{-1} in the cocrystal, which can sharply slow down the nonradiative decay.[30] Meanwhile, the reorganization energies for $S_1 \rightarrow T_1$ and $S_1 \rightarrow T_2$ remain similar in the three phases, indicating similar behavior for k_{ISC}. We thus conclude that the strong hydrogen bonding can suppress the nonradiative decay of $T_1 \rightarrow S_0$ by vibronic decoupling for the triplet state with (π, π^*) character, allowing bright and long-lived RTP in the Cz2BP cocrystal. This mechanism has been successfully applied to realize the control of emission behavior from phosphorescence to fluorenscence by tuning the substitution from fluoro to hydrogen and then to the hydroxyl group for a series of carbazole-based emitters.[48]

https://dx.doi.org/10.1021/acs.accounts.0c00556
Acc. Chem. Res. 2021, 54, 940−949

2.3. π−Halogen-Bonding-Enhanced k_{ISC} through Strengthening the SOC

The π−halogen bond is one type of halogen bond (XB) which is formed between a covalently bonded halogen atom (e.g., C−X, X = Cl, Br, I; X^-; XB donor) and a nucleophile (e.g., C−Y, Y = O, N, S; aryl π; XB acceptor). The π−halogen interactions have attracted increasing attention owing to the molecular recognition in chemical and biological systems, which contribute greatly to the high binding affinity in drug design and lead optimization.[49−52] On the basis of the statistical data derived from 189 distinct X-attention π interactions in 146 protein structures, the π−halogen bond satisfies the following criteria among the distances d (X−centroid) and the angles α and θ as shown in Figure 5a: d (Cl−centroid) < 4.2 Å, d (Br−centroid) < 4.3 Å, and d (I−centroid) < 4.5 Å, as well as α < 60° and θ > 120°.[52] It is intriguing to investigate the π−halogen interaction effects on the photophysical property in organic molecules.

o-BrTCz and *m*-BrTCz (**18** and **19** in Figure 2) are a pair of isomers which differ only in halogen substitution positions but exhibit different ultralong phosphorescence with distinctly different quantum efficiencies of 2.3 and 13%, respectively, under ambient conditions in crystalline phases.[32] Comparing the X-ray single-crystal structures of the two compounds as shown in Figure 5b,c, we find that there are two kinds of intermolecular hydrogen bonds, C−Br···H−C, and halogen bonds, C−Br···π. The C−Br···H−C distances of the isomers are close to each other, with 3.100 Å for molecule **19** and 2.963 Å for molecule **18**, respectively. In contrast, the distance for C−Br···π in the molecule **19** crystal (3.461 Å) is much shorter than that in the molecule **18** crystal (3.805 Å). Moreover, the $\alpha_{C-Br\cdots\pi}$ value of molecule **19** (26.7°) is smaller than 60°, while that in the molecule **18** crystal (90°) is larger than 60°. These structure differences indicate that the π−halogen interactions in molecule **19** are stronger than in molecule **18** crystals. To understand the influence of the π−halogen bonding interaction on the phosphorescence process, we built the computational models of a monomer with Br−H where Br stems from the nearest-neighbor molecule and Br−H is used to fix the direction of the Br−C bond in the whole molecule. This simplified model not only reduces the computational load but also excludes the effect of other factors (e.g., π−π stacking). The electronic structures of the low-lying excited states were calculated via TD-B3LYP/6-31G(d) implemented in the BDF package,[44,45] and the results are shown in Figure 5b,c. It is seen that there are six triplet states below the S_1 in energy for molecules **18** and **19** with similar singlet−triplet energy gaps. Compared to the SOC of the two compounds, it is found that the SOC between S_1 and $T_{n\ (n\leq 6)}$ of molecule **19** is always larger than the counterpart of molecule **18**. In particular, the SOC between S_1 and T_6 of molecule **19** (1.36 cm^{-1}), which is the closest triplet state to S_1, is larger by 1 order of magnitude than that of molecule **18** (0.10 cm^{-1}). We plot the transition property of T_6 upon excitation and surprisingly find that the Br atom makes many more contributions to the natural transition orbital (NTO) in molecule **19** than to that in molecule **18**. Note that the Br atom comes from the neighboring molecule. That is, the intermolecular C——Br···π halogen bond interaction in molecule **19** induces more participation of the Br atom in the low-lying triplet states and facilitates the ISC process, which generates a larger amount of spin−orbit coupling owing to the heavy-atom effect, thus facilitating the ISC process. These rationalize the observed higher phosphorescence efficiency of molecule **19** compared to that of molecule **18**.

A second example for the π−halogen-bond-induced RTP is in organic salt crystal TPO-Br (**20** in Figure 2) with a Br anion and aromatic π^+.[33] We built a computational model with the central molecule as the QM part and the surroundings as MM. The S_0 geometry is optimized and the excitation energies and transition properties of the low-lying excited states are evaluated at the level of ONIOM(B3LYP/6-311 G(d)/UFF) with the Gaussian 09 package.[53] The SOCs between singlet and triplet states are computed with the BDF package,[44,45] as shown in Figure 5d. The Br anion−π^+ interaction induces the participation of the Br anion in the excited-state structures as indicated by NTO analysis for molecule **20**. The resulting SOC between S_1 and $T_{n>1}$ is enhanced by 3 orders of magnitude to 450.39 cm^{-1}. The experimental phosphorescence quantum yield of the TPO-Br single crystal was found to be 36.56%. Thus, halogen anion−π^+ interactions can be a facile strategy for constructing RTP-active organic salt compounds.

3. MOLECULAR DESCRIPTORS TO CHARACTERIZE THE PHOSPHORESCENCE EFFICIENCY AND LIFETIME

To acquire a highly efficient RTP, it is necessary to open up efficient ISC processes from S_1 to T_n (T_n could be a little bit higher than T_1) and to slow down the nonradiative decays from S_1/T_1 to S_0, which could be realized in a rigid aggregation environment.[5] Except for a long-lived RTP, it is required to slow down the phosphorescent radiative decay k_P from T_1 to S_0. By virtue of the El-Sayed rules,[54] the ISC rate becomes relatively large if the initial and final states have different electronic compositions, for example, between (n → π^*) and (π → π^*) states, as in molecules combining lone-pair electrons in the n groups and π groups.[3]

Thus, we choose molecules with carbonyl groups (C═O) to produce n orbitals coupled with various conjugated π groups to introduce π orbitals, namely, BP (**3**), DFBP (**4**), FBDBF (**12**), *m*FDBP (**14**), BDBF (**15**), *p*DBP (**16**), and benzil (**17**) as shown in Figure 2. We first performed DFT and TDDFT calculations at the B3LYP/6-31G(d, p) level with the *Gaussian 09* package, and then we examined the relationship between the proportions of electronic composition (n, π^*) and (π, π^*) with respect to SOC constant ξ and the experimental phosphorescence lifetime τ_P as depicted in Figure 6. The singlet/triplet excited state can be regarded as an admixture of (n, π^*) and (π, π^*) configurations with portions α and β; that is, S/T = α(n, π^*) + β(π, π^*) with α + β = 1, and the difference in configuration between the S_1 and T_n states is expressed by $\Delta\alpha_n = |\alpha_{n,S_1} - \alpha_{n,T_1}|$. From Figure 6, it can be seen that ξ and $\Delta\alpha_{ns}$ have a strong monotonic correlation, which can be identified as an indicator of RTP efficiency. And a large value of β calculated for the T_1 state indeed correlates well with the long τ_P from experiments. For example, molecules **3**, **4**, and **17** have a short τ_P of microseconds owing to their small β value of <50%, and molecules **14**−**16** show long-lived phosphorescence for their large β value of >70%. Excitingly, molecule **15** possesses a typical ^{1}(n, π^*) S_1 state, a low-lying hybrid ^{3}(n, π^*) and ^{3}(π, π^*) T_2 state, and a typical ^{3}(π, π^*) T_1 state. This combination results in a large value of $\Delta\alpha_n$ between S_1 and T_2 to open up a significantly fast S_1 → T_2 ISC channel for high Φ_P and a large value of β in T_1 to slow down k_P and $k_{nr}^{T_1}$, which are shut down for long τ_P,

https://dx.doi.org/10.1021/acs.accounts.0c00556
Acc. Chem. Res. 2021, 54, 940−949

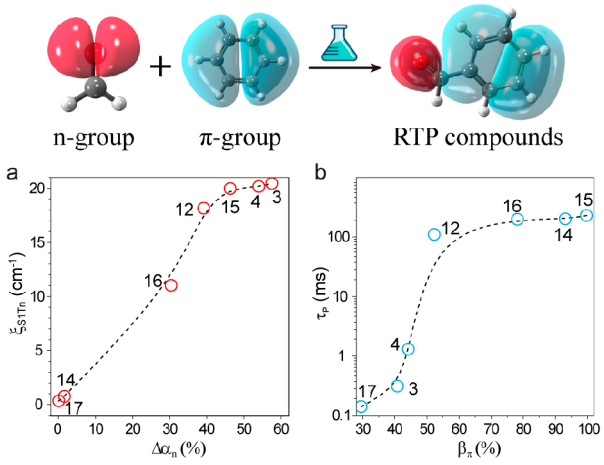

Figure 6. (a) Relationship between the SOC constant (ξ) and the difference in the proportion of the (n, π^*) configuration ($\Delta\alpha_n$) between S_1 and T_n by TD-DFT calculations. (b) Plot of the experimental phosphorescence lifetime (τ_P) against the proportion of the (π, π^*) configuration (β) in the T_1 state. Reproduced with permission from ref 3. Copyright 2016 Elsevier Inc.

which agrees well with its high efficency of up to 34.5% and ultralong lifetime of up to 0.23 s in the experiment. Thus, the experimental data prove that a balanced lifetime and efficiency of RTP can be realized by tuning the features of the molecular orbital and the energy level of the excited states via tailoring the aromatic subunits.

A variety of organic RTP systems have been found and synthesized because people have paid quite a bit of attention to this issue, including carbazole, a triazine derivative, and carbonyl compounds as shown in Figure 2. Among these compounds, the π-conjugated ones exhibit ultralong phosphorescence but an extremely low efficiency of <5%[4,10,14] (e.g., molecules **1** and **2**). The typical n-group compounds are well known to have highly efficient RTP values but short lifetimes on the order of microseconds[13] (e.g., molecule **4**). For similar aromatic carbonyl compounds containing n/π groups, their lifetimes vary over a wide range from 0.12 ms to 1.36 s, and their Φ_P values are changed from an extremely low 0.4% to a high 34.5%[19,22,55−58] At first glance, there are not any regularities to follow for the relationship between lifetime/efficiency and molecular structure because all of the compounds contain heteroatoms with lone-pair electrons.

To determine the inherent rules, we further improved the physical parameters to describe the change in the molecular configurations and establish the relationship between the descriptors and the quantum efficiency and lifetime of RTP. On the basis of the one-electron orbital approximation, the SOC between S_1 and T_n can be simply expressed as

$$\langle S_1|\hat{H}_{SOC}|T_n\rangle \propto {}^S\langle n + \pi|L|n + \pi\rangle^T$$
$$= {}^S\langle n|L|\pi\rangle^T + {}^S\langle \pi|L|n\rangle^T + {}^S\langle n|L|n\rangle^T + {}^S\langle \pi|L|\pi\rangle^T$$
$$\approx \alpha^S\cdot\beta^T + \beta^S\cdot\alpha^T = \gamma \quad (3)$$

Herein, the terms with the same n or π orbitals between the S and T states are banished. The γ is the orbital overlap integral for these two states after considering the spin and orbital interaction, which is a better indicator of the SOC strength between them. Similarly, the SOC between T_1 and S_0 is

$$\langle T_1|\hat{H}_{SOC}|S_0\rangle \propto \alpha^T = 1 - \beta^T \quad (4)$$

As is well known, the ISC rate is mainly determined by the SOC and the energy gap (ΔE_{ST}) between the S and T states, and strengthening the SOC and lowering the ΔE_{ST} can fasten the k_{ISC}. Thus, the ISC process of $S_1 \rightarrow T_n$ with the smallest ΔE_{ST} always acts as the most dominant one among the triplet states lying lower than S_1 in energy. In such a case, the ISC rate can be mainly governed by the γ value of the significant $S_1 \rightarrow T_n$, and that of $T_1 \rightarrow S_0$ can be estimated by the α or β value of T_1. After combining eqs 1−4, we conclude that phosphorescence Φ_P and τ_P values can be crudely proportional to the γ value of $S_1 \rightarrow T_n$ and the β value of T_1, respectively.[4]

We performed QM/MM calculations with the TD/B3LYP/6-31G (d, p)/GAFF method by using the ChemShell 3.5 packages interfacing Turbomole 6.5 for QM and DL_POLY for MM, and we plotted the curves of the calculated γ and β values versus the measured Φ_P and τ_P values in Figure 7,

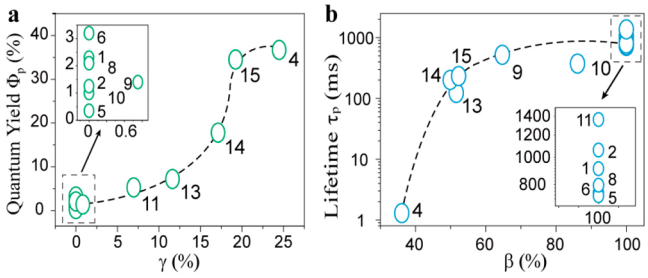

Figure 7. Relationship between the phosphorescence quantum yield (Φ_P), lifetime (τ_P), and pair descriptors (γ, β). Reproduced with permission from ref 4. Copyright 2019 American Chemical Society.

respectively, for compounds **1**−**12** in the crystalline phase. Excitingly, it is found that Φ_P is gradually enhanced from 0.4 to 34.5% as the γ value increases from 0.0 to 24.5%. There are some exceptions (molecules **1**−**2** and **4**−**8**) because its γ values are very small, <1.0%, resulting in indistinguishably low Φ_P values of <3.0% (inset in Figure 7). Similarly, the τ_P is prolonged with the increase in the β value in general, although molecules **1**, **2**, **5**, **6**, **8**, and **11** exhibit different τ_P values from 730 to 1360 ms for the same β value of 100.0%. It can be easily understood from the deviations of Φ_P and τ_P that the ISC rate is related not only to electronic properties SOC and ΔE but also to the vibrational structure and electron−vibration coupling,[3,39] which is neglected here. In a word, the changes in Φ_P and τ_P can be determined by the pair descriptors (γ, β) to a large extent. This also explains the fact that the introduction of the carbonyl group in molecules **4**−**8** cannot promote Φ_P because of their very small γ values. Most importantly, the organic compounds containing n/π groups with rational molecular design are favorable for the enlargement of γ and β values, thus facilitating RTP in organic molecules with high efficiency and a long-lived afterglow simultaneously.

The design strategy for balancing the efficiency and lifetime of phosphorescence by adjusting the appreciable proportion of (π, π^*) and (n, π^*) in the electronic configuration has been successfully used in experiments. For instance, on the basis of the SPh compound, Chi et al. designed and synthesized OMe-SPhT with a high efficiency and a long lifetime by balancing the (π, π^*) and (n, π^*) components, which were verified via single-crystal X-ray diffraction analysis and theoretical

https://dx.doi.org/10.1021/acs.accounts.0c00556
Acc. Chem. Res. 2021, 54, 940−949

calculations.[59] In addition, the pair of descriptors is also expected to be used for large-scale molecular screenings of the RTP materials.

4. CONCLUSIONS AND PERSPECTIVES

The mechanism of RTP in organic aggregates and the design strategy of highly efficient long-lived RTP material have been extensively unraveled through systematical calculations and analyses for all of the involved dynamic processes (k_F, k_P, $k_{nr}^{S_1}$, k_{ISC}, and $k_{nr}^{T_1}$) and molecular structure parameters, including the electronic configuration of the excited states, spin−orbit coupling, and vibrational-mode-induced nonadiabatic coupling. As the most fundamental element, the electronic configuration of an excited state is determined by the chemical structure, which is subject to the aggregation structure. The (n, π^*) configuration is more sensitive to the electrostatic interaction than the (π, π^*) one; namely, the former is usually destabilized and the latter undergoes a slight change in energy by the electrostatic interaction. Therefore, the occurrence of RTP stems from the change in k_P, $k_{nr}^{S_1}$, k_{ISC}, or $k_{nr}^{T_1}$, which is strongly molecular-structure-dependent and aggregation-topology-dependent, as revealed by the QM/MM calculations. These findings open up more innovative space to design high-efficiency RTP material.

Taking n groups connected to π groups as a molecular model, we proposed the molecular design strategy to balance the efficiency and lifetime of phosphorescence by adjusting the appreciable proportion of (n, π^*) and (π, π^*) in the electronic configuration and established a pair of molecular electronic configuration descriptors (γ, β) to characterize the phosphorescence efficiency and lifetime, respectively. Both the phosphorescence efficiency and lifetime are promoted by the increase in the γ and β values. As expected, the organic compounds containing n/π groups with rational molecular design are favorable to the increase in γ and β values, thus facilitating RTP in organic molecules with high efficiency and long-lived afterglow simultaneously. This design strategy has been successfully used in experiments. The pair of molecular descriptors is believed to be helpful for the future design of machine-learning-based high-efficiency, purely RTP materials.

So far, we have investigated the photophysical behavior of a single molecule embedded in a frozen surrounding environment. We have overlooked some other intermolecular deactivation processes, such as energy transfer and charge transfer. We have discussed only for the properties of the molecules at the equilibrium geometry of the potential energy surfaces, which excluded the deformation of potential energy surfaces effects, such as the photoisomerization and crossing points and so on. In addition, for the key ISC processes, the contribution of intermediate states to the ISC rate has not been considered, which is regarded to be very important in some organic systems. Very recently, novel RTP phenomena are continuously discovered and reported, such as cluster-induced RTP of nonconjugated molecules,[60] mechanochromic RTP of organic molecules,[17] multicolor RTP of a single molecule,[61] dynamic ultralong RTP by photoactivation,[62] RTP caused by chromophore-solvent reaction,[63] singlet-fission-caused RTP,[64] and so on beyond the conventional organic photophysics scenarios. The mechanisms of organic phosphorescence stemming from impurities in many solid organic compounds were reported almost a century ago[65] and have not been made clear until now. All of these issues require further revealing the mechanisms behind the new luminescence behaviors from a brand new theoretical perspective. Therefore, this field is full of challenges and opportunities in the future.

AUTHOR INFORMATION

Corresponding Author

Zhigang Shuai − *MOE Key Laboratory of Organic OptoElectronics and Molecular Engineering, Department of Chemistry, Tsinghua University, Beijing 100084, P. R. China;* orcid.org/0000-0003-3867-2331; Phone: +86-10-62797689; Email: zgshuai@tsinghua.edu.cn

Authors

Qian Peng − *School of Chemical Sciences, University of Chinese Academy of Sciences, 100049 Beijing, P. R. China; Key Laboraorty of Organic Solids, Institute of Chemistry of the Chinese Academy of Sciences, 100190 Beijing, P. R. China;* orcid.org/0000-0001-8975-8413

Huili Ma − *Key Laboratory of Flexible Electronics (KLOFE) & Institute of Advanced Materials (IAM), Nanjing Tech University (NanjingTech), Nanjing 211816, P. R. China;* orcid.org/0000-0003-0332-2999

Complete contact information is available at: https://pubs.acs.org/10.1021/acs.accounts.0c00556

Notes

The authors declare no competing financial interest.

Biographies

Qian Peng received her Ph.D. from the Institute of Chemistry of the Chinese Academy of Sciences in 2008 supervised by Prof. Z. Shuai. Then she joined the Key Laboratory of Organic Solids at the Institute as a research assistant, and she was promoted to associate professor in 2010 and full professor in 2019 there. In 2020, she joined the School of Chemical Sciences, University of Chinese Academy of Sciences in Beijing. Her research interests are theoretical investigations into the molecular aggregation effects on the light-emitting phenomena with excited-state decay processes involving nonadiabatic and spin−orbit couplings, photophysical mechanisms of various luminescence phenomena in organic optoelectronic materials, and the theoretical design of light-emitting molecules.

Huili Ma received his Ph.D. from the University of Science and Technology of China under the supervision of Prof. Wanzhen Liang in 2014. He then worked as a postdoctoral researcher with Prof. Z. Shuai at Tsinghua University. In 2018, he joined Nanjing Tech University, where he is now an associate professor. His research interests focus on the theory and simulation of organic luminescent materials with a strong focus on organic RTP phenomena.

Zhigang Shuai received his Ph.D. in theoretical physics from Fudan University in 1989. He accepted a full professor position in the Hundred-Talent Program in 2000 at the Institute of Chemistry of the Chinese Academy of Sciences after working as postdoctoral researcher and research scientist for 11 years at the University of Mons, Belgium. He moved to Tsinghua University as a Changjiang Scholar Professor in 2008. His research interests focus on the development and application of theoretical modeling methods for the electronic processes in organic optoelectronic materials.

ACKNOWLEDGMENTS

This work is supported by the National Natural Science Foundation of China (grant nos. 21788102, 21973099, and 21973043) and the Ministry of Science and Technology of

China through the National Key R&D Plan (grant no. 2017YFA0204501). Stimulating discussions and collaborations with Profs. B. Z. Tang, W. Huang, Z. Li, A. J. Qin, Z. F. An, X. G. Gu, and more are greatly acknowledged.

REFERENCES

(1) Ma, H.; Shi, W.; Ren, J.; Li, W.; Peng, Q.; Shuai, Z. Electrostatic Interaction-Induced Room-Temperature Phosphorescence in Pure Organic Molecules from QM/MM Calculations. *J. Phys. Chem. Lett.* **2016**, *7*, 2893−2898.
(2) Ma, H.; Yu, H.; Peng, Q.; An, Z.; Wang, D.; Shuai, Z. Hydrogen Bonding-Induced Morphology Dependence of Long-Lived Organic Room-Temperature Phosphorescence: A Computational Study. *J. Phys. Chem. Lett.* **2019**, *10*, 6948−6954.
(3) Zhao, W.; He, Z.; Lam, J.; Peng, Q.; Ma, H.; Shuai, Z.; Bai, G.; Hao, J.; Tang, B. Rational Molecular Design for Achieving Persistent and Efficient Pure Organic Room-Temperature Phosphorescence. *Chem.* **2016**, *1*, 592−602.
(4) Ma, H.; Peng, Q.; An, Z.; Huang, W.; Shuai, Z. Efficient and Long-Lived Room-Temperature Organic Phosphorescence: Theoretical Descriptors for Molecular Designs. *J. Am. Chem. Soc.* **2019**, *141*, 1010−1015.
(5) Mei, J.; Leung, N.; Kwok, R.; Lam, J.; Tang, B. Aggregation-induced emission: together we shine, united we soar! *Chem. Rev.* **2015**, *115*, 11718−11940.
(6) Xu, S.; Chen, R.; Zheng, C.; Huang, W. Excited State Modulation for Organic Afterglow: Materials and Applications. *Adv. Mater.* **2016**, *28*, 9920.
(7) Fateminia, S.; Mao, Z.; Xu, S.; Yang, Z.; Chi, Z.; Liu, B. Organic Nanocrystals with Bright Red Persistent Room-Temperature Phosphorescence for Biological Applications. *Angew. Chem., Int. Ed.* **2017**, *56*, 12160.
(8) Zhang, G.; Palmer, G.; Dewhirst, M.; Fraser, C. A dual-emissive-materials design concept enables tumour hypoxia imaging. *Nat. Mater.* **2009**, *8*, 747−751.
(9) Li, Y.; Gecevicius, M.; Qiu, J. Long Persistent Phosphors-from Fundamentals to Applications. *Chem. Soc. Rev.* **2016**, *45*, 2090.
(10) Turro, N. J.; Ramamurthy, V.; Scaiano, J. C. *Modern Molecular Photochemistry of Organic Molecules*; Viva Books, University Science Books: Sausalito, 2017.
(11) Bilen, C.; Harrison, N.; Morantz, D. Unusual room temperature afterglow in some crystalline organic compounds. *Nature* **1978**, *271*, 235.
(12) Schulman, E.; Walling, C. Phosphorescence of adsorbed ionic organic molecules at room temperature. *Science* **1972**, *178*, 53−54.
(13) Yuan, W.; Shen, X.; Zhao, H.; Lam, J.; Tang, L.; Lu, P.; Wang, C.; Liu, Y.; Wang, Z.; Zheng, Q.; Sun, J.; Ma, Y.; Tang, B. Crystallization-Induced Phosphorescence of Pure Organic Luminogens at Room Temperature. *J. Phys. Chem. C* **2010**, *114*, 6090−6099.
(14) An, Z.; Zheng, C.; Tao, Y.; Chen, R.; Shi, H.; Chen, T.; Wang, Z.; Li, H.; Deng, R.; Liu, X.; Huang, W. Stabilizing triplet excited states for ultralong organic phosphorescence. *Nat. Mater.* **2015**, *14*, 685−690.
(15) Kabe, R.; Adachi, C. Organic Long Persistent Luminescence. *Nature* **2017**, *550*, 384.
(16) Ma, X.; Wang, J.; Tian, H. Assembling-Induced Emission: An Efficient Approach for Amorphous Metal-Free Organic Emitting Materials with Room-Temperature Phosphorescence. *Acc. Chem. Res.* **2019**, *52*, 738−748.
(17) Li, Q.; Li, Z. Molecular Packing: Another Key Point for the Performance of Organic and Polymeric Optoelectronic Materials. *Acc. Chem. Res.* **2020**, *53*, 962−973.
(18) Bolton, O.; Lee, K.; Kim, H.; Lin, K.; Kim, J. Activating efficient phosphorescence from purely organic materials by crystal design. *Nat. Chem.* **2011**, *3*, 205−210.
(19) Xie, Y.; Ge, Y.; Peng, Q.; Li, C.; Li, Q.; Li, Z. How the Molecular Packing Affects the Room Temperature Phosphorescence in Pure Organic Compounds: Ingenious Molecular Design, Detailed Crystal Analysis, and Rational Theoretical Calculations. *Adv. Mater.* **2017**, *29*, 1606829.
(20) Yang, J.; Zhen, X.; Wang, B.; Gao, X.; Ren, Z.; Wang, J.; Xie, Y.; Li, J.; Peng, Q.; Pu, K.; Li, Z. The influence of the molecular packing on the room temperature phosphorescence of purely organic luminogens. *Nat. Commun.* **2018**, *9*, 840.
(21) Yang, J.; Ren, Z.; Chen, B.; Fang, M.; Zhao, Z.; Tang, B.; Peng, Q.; Li, Z. Three polymorphs of one luminogen: how the molecular packing affects the RTP and AIE properties? *J. Mater. Chem. C* **2017**, *5*, 9242−9246.
(22) Li, C.; Tang, X.; Zhang, L.; Li, C.; Liu, Z.; Bo, Z.; Dong, Y. Q.; Tian, Y.-H.; Dong, Y.; Tang, B. Z. Reversible Luminescence Switching of an Organic Solid: Controllable On-Off Persistent Room Temperature Phosphorescence and Stimulated Multiple Fluorescence Conversion. *Adv. Opt. Mater.* **2015**, *3*, 1184.
(23) Wang, J.; Chai, Z.; Wang, J.; Wang, C.; Han, M.; Liao, Q.; Huang, A.; Lin, P.; Li, C.; Li, Q.; Li, Z. Mechanoluminescence or Room Temperature Phosphorescence: Molecular Packing-Dependent Emission Response. *Angew. Chem., Int. Ed.* **2019**, *58*, 17297−17302.
(24) Singh, N. J.; Min, S. K.; Kim, D. Y.; Kim, K. S. Comprehensive energy analysis for various types of π-interaction. *J. Chem. Theory Comput.* **2009**, *5*, 515−529.
(25) Sherrill, C. Energy Component Analysis of π Interactions. *Acc. Chem. Res.* **2013**, *46*, 1020−1028.
(26) Emamian, S.; Lu, T.; Kruse, H.; Emamian, H. Exploring Nature and Predicting Strength of Hydrogen Bonds: A Correlation Analysis Between Atoms-in-Molecules Descriptors, Binding Energies, and Energy Components of Symmetry-Adapted Perturbation Theory. *J. Comput. Chem.* **2019**, *40*, 2868−2881.
(27) Yang, L.; Wang, X.; Zhang, G.; Chen, X.; Zhang, G.; Jiang, J. Aggregation-induced intersystem crossing: a novel strategy for efficient molecular phosphorescence. *Nanoscale* **2016**, *8*, 17422−17426.
(28) Ma, H.; Lv, A.; Fu, L.; Wang, S.; An, Z.; Shi, H.; Huang, W. Room Temperature Phosphorescence in Metal Free Organic Materials. *Ann. Phys.* **2019**, *531*, 1800482.
(29) Shuai, Z.; Peng, Q. Organic light-emitting diodes: theoretical understanding of highly efficient materials and development of computational methodology. *Natl. Sci. Rev.* **2017**, *4*, 224−239.
(30) Zhang, T.; Jiang, Y. Q.; Niu, Y. L.; Peng, Q.; Shuai, Z. Aggregation Effects on the Optical Emission of 1,1,2,3,4,5-Hexaphenylsilole (HPS): A QM/MM Study. *J. Phys. Chem. A* **2014**, *118*, 9094−9104.
(31) Zhang, T.; Peng, Q.; Quan, C.; Nie, H.; Niu, Y.; Xie, Y.; Zhao, Z.; Tang, B.; Shuai, Z. Using the isotope effect to probe an aggregation induced emission mechanism: theoretical prediction and experimental validation. *Chem. Sci.* **2016**, *7*, 5573−5580.
(32) Cai, S.; Shi, H.; Tian, D.; Ma, H.; Cheng, Z.; Wu, Q.; Gu, M.; Huang, L.; An, Z.; Peng, Q.; Huang, W. Enhancing Ultralong Organic Phosphorescence by Effective π-Type Halogen Bonding. *Adv. Funct. Mater.* **2018**, *28*, 1705045.
(33) Wang, J.; Gu, X.; Ma, H.; Peng, Q.; Huang, X.; Zheng, X.; Sung, S.; Shan, G.; Lam, J.; Shuai, Z.; Tang, B. A facile strategy for realizing room temperature phosphorescence and single molecule white light emission. *Nat. Commun.* **2018**, *9*, 2963.
(34) Shuai, Z.; Wang, D.; Peng, Q.; Geng, H. Computational evaluation of optoelectronic properties for organic/carbon materials. *Acc. Chem. Res.* **2014**, *47*, 3301−3309.
(35) Gong, Y.; Zhao, L.; Peng, Q.; Fan, D.; Yuan, W.; Zhang, Y.; Tang, B. Crystallization-induced dual emission from metal- and heavy atom-free aromatic acids and esters. *Chem. Sci.* **2015**, *6*, 4438−4444.
(36) Ahlrichs, R.; Bär, M.; Häser, M.; Horn, H.; Kölmel, C. Electronic Structure Calculations on Workstation Computers: The Program System Turbomole. *Chem. Phys. Lett.* **1989**, *162*, 165−169.
(37) Aquilante, F.; De Vico, L.; Ferré, N.; Ghigo, G.; Malmqvist, P.å.; Neogrády, P.; Pedersen, T.; Pitonák, M.; Reiher, M.; Roos, B. O.; Serrano-Andrés, L.; Urban, M.; Veryazov, V.; Lindh, R. MOLCAS 7: The Next Generation. *J. Comput. Chem.* **2010**, *31*, 224−247.

https://dx.doi.org/10.1021/acs.accounts.0c00556
Acc. Chem. Res. 2021, 54, 940−949

(38) Moyna, G.; Williams, H.; Nachman, R.; Scott, A. Conformation in Solution and Dynamics of a Structurally Constrained inear Insect Kinin Pentapeptide Analogue. *Biopolymers* **1999**, *49*, 403−413.
(39) Peng, Q.; Niu, Y.; Shi, Q.; Gao, X.; Shuai, Z. Correlation function formalism for triplet excited state decay: combined spin-orbit and non-adiabatic couplings. *J. Chem. Theory Comput.* **2013**, *9*, 1132−1143.
(40) Hirata, S. Intrinsic Analysis of Radiative and Room-Temperature Nonradiative Processes Based on Triplet State Intramolecular Vibrations of Heavy Atom-Free Conjugated Molecules toward Efficient Persistent Room-Temperature Phosphorescence. *J. Phys. Chem. Lett.* **2018**, *9*, 4251−4259.
(41) Beran, G. Modeling Polymorphic Molecular Crystals with Electronic Structure Theory. *Chem. Rev.* **2016**, *116*, 5567−5613.
(42) Sherwood, P.; de Vries, A.; Guest, M.; Schreckenbach, G.; Catlow, C.; French, S.; Sokol, A.; Bromley, S.; Thiel, W.; Turner, A. J.; Billeter, S.; Terstegen, F.; Thiel, S.; Kendrick, J.; Rogers, S. C.; Casci, J.; Watson, M.; King, F.; Karlsen, E.; Sjøvoll, M.; Fahmi, A.; Schäfer, A.; Lennartz, C. QUASI: A general purpose implementation of the QM/MM approach and its application to problems in catalysis. *J. Mol. Struct.: THEOCHEM* **2003**, *632*, 1−28.
(43) Smith, W.; Forester, T. DL_POLY_2.0: A general-purpose parallel molecular dynamics simulation package. *J. Mol. Graphics* **1996**, *14*, 136−141.
(44) Li, Z.; Xiao, Y.; Liu, W. On the spin separation of algebraic two-component relativistic Hamiltonians. *J. Chem. Phys.* **2012**, *137*, 154114.
(45) Zhang, Y.; Suo, B. B.; Wang, Z. K.; Zhang, N.; Li, Z. D.; Lei, Y. B.; Zou, W. L.; Gao, J.; Peng, D. L.; Pu, Z. C.; Xiao, Y. L.; Sun, Q. M.; Wang, F.; Ma, Y. T.; Wang, X. P.; Guo, Y.; Liu, W. J. *J. Chem. Phys.* **2020**, *152*, 064113.
(46) Shuai, Z. Thermal vibration correlation function formalism for molecular excited state decay rates. *Chin. J. Chem.* **2020**, *38*, 1223−1232.
(47) Niu, Y.; Li, W.; Peng, Q.; Geng, H.; Yi, Y.; Wang, L.; Nan, G.; Wang, D.; Shuai, Z. Molecular Materials Property Prediction Package (MOMAP) 1.0: a software package for predicting the luminescent properties and mobility of organic functional materials. *Mol. Phys.* **2018**, *116*, 1078−1090.
(48) Feng, H.; Zeng, J.; Yin, P.; Wang, X.; Peng, Q.; Zhao, Z.; Lam, J.; Tang, B. Tuning molecular emission of organic emitters from fluorescence to phosphorescence through push-pull electronic effects. *Nat. Commun.* **2020**, *11*, 2617.
(49) Xu, Z.; Yang, Y.; Liu, Y.; Lu, Y.; Chen, K.; Zhu, W. Halogen Bond: Its Role beyond Drug-Target Binding Affinity for Drug Discovery and Development. *J. Chem. Inf. Model.* **2014**, *54*, 69−78.
(50) Matter, H.; Nazaré, M.; Güssregen, S.; Will, D. W.; Schreuder, H.; Bauer, A.; Urmann, M.; Ritter, K.; Wagner, M.; Wehner, V. Evidence for C-Cl/C-Br···/ Interactions as an Important Contribution to Protein-Ligand Binding Affinity. *Angew. Chem., Int. Ed.* **2009**, *48*, 2911−2916.
(51) Sun, H.; Horatscheck, A.; Martos, V.; Bartetzko, M.; Uhrig, U.; Lentz, D.; Schmieder, P.; Nazar, M. Direct Experimental Evidence for Halogen-Aryl A Interactions in Solution from Molecular Torsion Balances. *Angew. Chem., Int. Ed.* **2017**, *56*, 6454−6458.
(52) Lu, Y.; Wang, Y.; Zhu, W. Nonbonding interactions of organic halogens in biological systems: implications for drug discovery and biomolecular design. *Phys. Chem. Chem. Phys.* **2010**, *12*, 4543−4551.
(53) Frisch, M. J.; Trucks, G. W.; Schlegel, H. B.; Scuseria, G. E.; Robb, M. A.; Cheeseman, J. R.; Scalmani, G.; Barone, V.; Mennucci, B.; Petersson, G. A.; Nakatsuji, H.; Caricato, M.; Li, X.; Hratchian, H. P.; Izmaylov, A. F.; Bloino, J.; Zheng, G.; Sonnenberg, J. L.; Hada, M.; Ehara, M.; Toyota, K.; Fukuda, R.; Hasegawa, J.; Ishida, M.; Nakajima, T.; Honda, Y.; Kitao, O.; Nakai, H.; Vreven, T.; Montgomery, J. A., Jr.; Peralta, J. E.; Ogliaro, F.; Bearpark, M. J.; Heyd, J.; Brothers, E. N.; Kudin, K. N.; Staroverov, V. N.; Kobayashi, R.; Normand, J.; Raghavachari, K.; Rendell, A. P.; Burant, J. C.; Iyengar, S. S.; Tomasi, J.; Cossi, M.; Rega, N.; Millam, N. J.; Klene, M.; Knox, J. E.; Cross, J. B.; Bakken, V.; Adamo, C.; Jaramillo, J.; Gomperts, R.; Stratmann, R. E.; Yazyev, O.; Austin, A. J.; Cammi, R.; Pomelli, C.; Ochterski, J. W.; Martin, R. L.; Morokuma, K.; Zakrzewski, V. G.; Voth, G. A.; Salvador, P.; Dannenberg, J. J.; Dapprich, S.; Daniels, A. D.; Farkas Foresman, J. B.; Ortiz, J. V.; Cioslowski, J.; Fox, D. J. *Gaussian 09*; Gaussian, Inc.: Wallingford, CT, 2009.
(54) El-Sayed, M. Triplet State. Its Radiative and Nonradiative Properties. *Acc. Chem. Res.* **1968**, *1*, 8−16.
(55) Sun, C.; Ran, X.; Wang, X.; Cheng, Z.; Wu, Q.; Cai, S.; Gu, L.; Gan, N.; Shi, H.; An, Z.; Shi, H.; Huang, W. Twisted Molecular Structure on Tuning Ultralong Organic Phosphorescence. *J. Phys. Chem. Lett.* **2018**, *9*, 335.
(56) Gong, Y.; Chen, G.; Peng, Q.; Yuan, W. Z.; Xie, Y.; Li, S.; Zhang, Y.; Tang, B. Achieving Persistent Room Temperature Phosphorescence and Remarkable Mechanochromism from Pure Organic Luminogens. *Adv. Mater.* **2015**, *27*, 6195.
(57) Yang, Z.; Mao, Z.; Zhang, X.; Ou, D.; Mu, Y.; Zhang, Y.; Zhao, C.; Liu, S.; Chi, Z.; Xu, J.; Wu, Y.; Lu, P.; Lien, A.; Bryce, M. Intermolecular Electronic Coupling of Organic Units for Efficient Persistent Room-Temperature Phosphorescence. *Angew. Chem., Int. Ed.* **2016**, *55*, 2181.
(58) Xiong, Y.; Zhao, Z.; Zhao, W.; Ma, H.; Peng, Q.; He, Z.; Zhang, X.; Chen, Y.; He, X.; Lam, J. W. Y.; Tang, B. Designing Efficient and Ultralong Pure Organic Room-Temperature Phosphorescent Materials by Structural Isomerism. *Angew. Chem., Int. Ed.* **2018**, *57*, 7997.
(59) Chen, J.; Rahman, N.; Mao, Z.; Zhao, J.; Yang, Z.; Liu, S.; Zhang, Y.; Chi, Z. Achievement of persistent and efficient organic room-temperature phosphorescence with temperature-response by adjusting the proportion of excited-state configurations in coupled molecules. *J. Mater. Chem. C* **2019**, *7*, 8250.
(60) Wang, Q.; Dou, X.; Chen, X.; Zhao, Z.; Wang, S.; Wang, Y.; Sui, K.; Tan, Y.; Gong, Y.; Zhang, Y.; Yuan, W. Reevaluating the Protein Emission: Remarkable Visible Luminescence and Emissive Mechanism. *Angew. Chem., Int. Ed.* **2019**, *58*, 12667−12673.
(61) He, Z.; Zhao, W.; Lam, J.; Peng, Q.; Ma, H.; Liang, G.; Shuai, Z.; Tang, B. White Light Emission from a Single Organic Molecule with Dual Phosphorescence at Room Temperature. *Nat. Commun.* **2017**, *8*, 416.
(62) Gu, L.; Shi, H.; Gu, M.; Ling, K.; Ma, H.; Cai, S.; Song, L.; Ma, C.; Li, H.; Xing, G.; Hang, X.; Li, J.; Gao, Y.; Yao, W.; Shuai, Z.; An, Z.; Liu, X.; Huang, W. Dynamic Ultralong Organic Phosphorescence by Photoactivation. *Angew. Chem., Int. Ed.* **2018**, *57*, 8425−8431.
(63) Chen, B.; Huang, W.; Su, H.; Miao, H.; Zhang, X.; Zhang, G. An Unexpected Chromophore-Solvent Reaction Leads to Bicomponent Aggregation-Induced Phosphorescence. *Angew. Chem., Int. Ed.* **2020**, *59*, 10023−10026.
(64) Koch, M.; Perumal, K.; Blacque, O.; Garg, J.; Saiganesh, R.; Kabilan, S.; Balasubramanian, K.; Venkatesan, K. Metal free triplet phosphors with high emission efficiency and high tunability. *Angew. Chem., Int. Ed.* **2014**, *53*, 6378−6382.
(65) Clapp, D. B. The Phosphorescence of Tetraphenylmethane and certain related substances. *J. Am. Chem. Soc.* **1939**, *61*, 523−524.

https://dx.doi.org/10.1021/acs.accounts.0c00556
Acc. Chem. Res. 2021, 54, 940−949